JACS
JOURNAL OF THE AMERICAN CHEMICAL SOCIETY

Article

Photostable Voltage Sensitive Dyes Based on Simple, Solvatofluorochromic, Asymmetric Thiazolothiazoles

Nickolas Sayresmith, Anand Saminathan, Joshua K. Sailer, Shannon M. Patberg, Kristin Sandor, Yamuna Krishnan, and Michael G. Walter

J. Am. Chem. Soc., **Just Accepted Manuscript** • DOI: 10.1021/jacs.9b08959 • Publication Date (Web): 29 Oct 2019

is published by the American Chemical Society. 1155 Sixteenth Street N.W., Washington, DC 20036

Photostable Voltage Sensitive Dyes Based on Simple, Solvatofluorochromic, Asymmetric Thiazolothiazoles

Nickolas A. Sayresmith,[†] Anand Saminathan,[‡] Joshua K. Sailer,[†] Shannon M. Patberg,[†] Kristin Sandor,[†] Yamuna Krishnan,[‡] and Michael G. Walter[,†]*

[†]Department of Chemistry, University of North Carolina at Charlotte, Charlotte, NC, 28223,

[‡]Department of Chemistry, University of Chicago, and Grossman Institute of Neuroscience, Quantitative Biology and Human Behavior, University of Chicago, Chicago, IL 60637

*Michael.Walter@uncc.edu

ABSTRACT: A family of asymmetric thiazolo[5,4-d]thiazole (TTz) fluorescent dye sensors have been developed and their photophysical sensing properties are reported. The π-conjugated, TTz-bridged compounds are synthesized via a single-step, double condensation/oxidation of dithiooxamide and two different aromatic aldehydes: one with strong electron donating characteristics and one with strong electron accepting characteristics. The four reported dyes include electron donating moieties (N,N dibutylaniline and N,N diphenylaniline) matched with three different electron accepting moieties (pyridine, benzoic acid, and carboxaldehyde). The asymmetric TTz derivatives exhibit strong solvatofluorochromism with Stokes shifts between 2270 and 6050 cm^{-1} and transition dipole moments ($\Delta\mu$ = 13 – 18 D) that are among the highest reported for push-pull dyes. Fluorescence quantum yields are as high as 0.93 in nonpolar solvents and the fluorescence lifetimes (τ_F) vary from 1.50 to 3.01 ns depending on the solvent polarity. In addition, thermofluorochromic studies and spectrophotometric acid titrations were performed and indicate the possibility of using these dyes as temperature and/or acid sensors. In vitro cell studies indicate good cell membrane localization, insignificant cytotoxicity, promising voltage sensitivities, and photostabilities that are 4 times higher than comparable dyes. Their ease of synthesis and purification, remarkable photophysical properties, and chemically sensitive TTz π-bridge make these asymmetric dye derivatives attractive for environmental and biological sensing or similar molecular optoelectronic applications.

KEYWORDS: Thiazolo[5,4-d]thiazole, push-pull, asymmetric, fluorophores, sensitizers, solvent-dependent Stokes shift, cell membrane voltage sensing.

INTRODUCTION

Small molecule fluorophores are attractive molecular tools for environmental sensing applications and biosensing/bioimaging techniques due to their high microenvironmental sensitivity, selectivity, and temporal resolution.[1] Fluorescent molecules can either turn on/off their fluorescence or chromically shift their emission through the binding or interaction of various metal ions,[2-5] reactive oxygen species,[6] organic toxins,[7] or cell organelles/membranes;[8-9] and can greatly enhance cell fluorescence microscopic imaging.[10] Molecular sensors with large fluorescence Stokes shifts are advantageous for these applications due to a low overlap between excitation and emission.[8]

A large majority of these molecular derivatives are designed with push-pull (electron withdrawing and donating) functional groups positioned at either ends of a π-conjugated aromatic core, which facilitates intramolecular charge-transfer (ICT) properties in the excited state.[11-13] Such push-pull dyes typically exhibit strong solvatofluorochromism and high environmental sensitivity as a result of the spatially separated and strengthened excited-state dipole.[14-15] New push-pull fluorophore discoveries in this field are driven by efforts to enhance ICT character, and therefore, increase their efficacy for monitoring molecular interactions, processes, and other events which require high specificity and environmental sensitivity.

Highly fluorescent, thiazolo[5,4-d]thiazole (TTz) chromophores have recently emerged as an important class of multifunctional heterocyclic compounds.[16-19] Molecular materials containing the fused, bicyclic thiazole backbone have exhibited strong fluorescence and electrofluorochromism,[16] and have been used in a variety of applications such as light-harvesting dyes in photovoltaics,[20-25] redox flow batteries,[17] and molecular sensors.[19, 26] Additionally, polymers incorporating the TTz moiety exhibit efficient electronic communication for organic

field-effect transistors with high free charge carrier mobility and good optoelectronic tunability.[27-30] The rigidity of the TTz structure is especially attractive for molecular optoelectronics due to their high thermo-oxidative and photochemical stability.[25, 30] Surprisingly, there have been very few reports of asymmetric TTz materials even though there exists a high demand for tunable, push-pull, small molecular systems that can be incorporated into a conjugated polymer backbone, or also for use in molecular sensing applications. This is especially relevant for asymmetric dyes that have shown promising photophysical properties as light harvesting dyes in small molecule solar cells.[23, 31-35] One challenge to the synthesis of asymmetric TTzs is the fact that the typical reaction pathway for forming the bicyclic heterocycle requires two, immediately sequential condensation steps, such that the isolation of the singly condensed intermediate is unfeasible. As a consequence, the introduction of asymmetry in most previously reported asymmetric TTzs have required the derivatization of an initially symmetric TTz using post-synthetic, low selectivity, mono-halogenation/mono-deprotection and Pd cross-coupling reactions.[23, 32, 34, 36-38] To emphasize, such routes towards asymmetric TTzs use multiple synthetic steps, require a similar number of purification procedures, and often result in low overall yields.

In an effort to address some of these issues, we have developed a new family of highly fluorescent, solvatofluorochromic, push-pull TTz compounds that can be accessed using a simple, single-step reaction (**Figure 1a**).

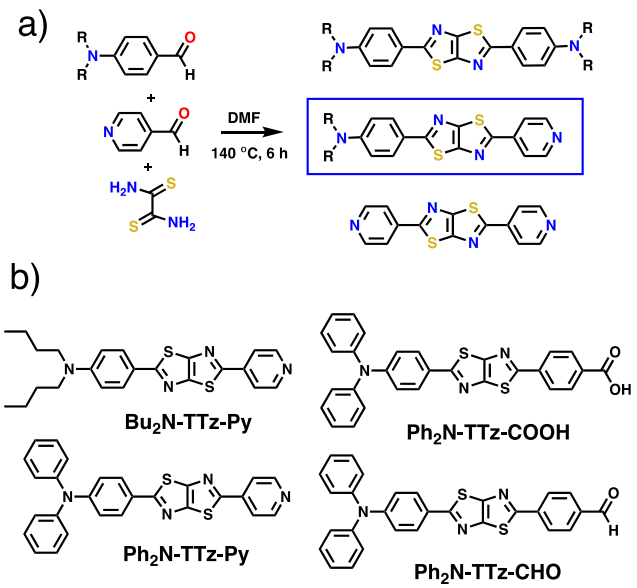

Figure 1. (a) Single step, synthetic reaction to form asymmetric TTz fluorophores and (b) the four asymmetric TTz compounds explored in this work.

The synthetic strategy begins by heating two different, readily available aromatic aldehyde precursors with dithiooxamide resulting in one asymmetric and two symmetric TTz chromophores. Judicious selection of the aromatic aldehyde precursors yields in an amphiphlic asymmetric TTz whose fluorescence on a column is uniquely distinguishable and whose column retention is intermediate that of its symmetric counterparts. In this way, silica gel chromatography gives an easily identifiable asymmetric TTz band (yellow fluorescence) in the middle of two spatially distant symmetric TTz bands (both with blue fluorescence). Four push-pull asymmetric TTz compounds were obtained in this manner (Bu_2N-TTz-Py, Ph_2N-TTz-Py, Ph_2N-TTz-COOH, and Ph_2N-TTz-CHO – **Figure 1b**) containing various electron-donating groups (dibutylamino, diphenylamino) and electron-withdrawing groups (pyridine, benzoic acid, and carboxaldehyde). The unique structural features of these chromophores compared to similar push-pull compounds composed of hydrocarbons is the highly fluorescent, electron deficient,

heterocyclic TTz bridge connecting the two asymmetric functional groups, whereby the lack of hydrogens in the TTz bridge allows for enhanced planarity by minimizing any steric effects typical of hydrocarbons.[9, 11-13] The rigid, fused-thiazole, bicyclic aromatic structure provides thermo-oxidative stability and the increased planarity further enhances the electronic interactions across the dye.[16] This means that compared to typical hydrocarbon-based, fluorescent biological dyes, the TTz dyes presented herein demonstrate much larger Stokes shifts, enhanced absorption coefficients, and red-shifted absorption and emission.[39] In addition, the thiazolothiazole bicyclic ring system provides further chemical functionality in a compact, π-conjugated bridge. All these properties make asymmetric TTzs a synthetically simple, photochemically attractive, and novel class of dyes suitable for environmental and biological sensing.

EXPERIMENTAL SECTION

Materials and Instrumentation. 4-pyridine carboxaldehyde, 4-(dibutylamino)benzaldehyde, 4-(diphenylamino)benzaldehyde, terephthalaldehyde, dithiooxamide, and all solvents used for spectroscopic measurements were purchased from Sigma-Aldrich and used without further purification. ^{1}H and ^{13}C NMR measurements were obtained with either a JEOL 300 MHz NMR or a JEOL 500 MHz NMR. High resolution mass spectra were obtained using a ThermoFisher Scientific MSQ Plus Single Quadrupole Mass Spectrometer. Solution-state UV-Vis spectra were collected on a Cary 300 UV-Vis spectrophotometer. Time-resolved measurements were taken on a Jobin Yvon-Spex Fluorolog equipped with a 389 nm diode laser for time-resolved PL decay measurements. Igor Pro 6.3 software was used to fit PL(t) decay data to single/multiple exponential decays. Quantum yields were calculated using 9,10-diphenylanthracene as a reference (quantum yield [Φ_F] in cyclohexanes = 0.97).[40-41] Density functional theory (DFT)

calculations were performed with Spartan computational software using B3LYP[42-43] density functional and 6-31G*[44] basis set. Temperature studies were conducted using a 10 μM Bu_2N-TTz-Py MeTHF solution placed inside of a Norrell 502 NMR tube and sequentially submerged in the following liquid N_2 baths: octanol (-16 °C), acetonitrile (-41 °C), acetone (-94 °C), pentane (-131 °C), MeTHF (-136 °C), and liquid N_2 itself (-196 °C). The phosphorescence spectrum of Bu_2N-TTz-Py (see S2) was collected similarly at -196 °C by pumping with 389 nm light while inside a liquid nitrogen bath and then probing the emission within 2 sec of removing from the bath. Human embryonic kidney cells (HEK 293T) were a kind gift from Prof. Bryan Dickinson, and Mouse macrophage J774A.1 cells were a kind gift from Prof. Deborah Nelson at the University of Chicago. Cells were cultured in Dulbecco's Modified Eagle's Medium (Invitrogen Corporation, USA) containing 10% heat inactivated Fetal Bovine Serum (FBS) (Invitrogen Corporation, USA), 100 U/mL penicillin, and 100 μg/mL streptomycin. Cells were maintained at 37 ºC under 5% CO_2.

Cell labeled spectral measurements. Excitation and emission spectra were collected by labeling the alveolar macrophage cell line J774.A1 (~ 0.5 x 10^5 cells) with 1 μM Bu_2N-TTz-Py in phosphate buffered saline (PBS) buffer and 0.1% TritonX-100. Cells were incubated with dye for 10 min at RT, washed thrice with PBS, and dispersed in a cuvette for fluorescent spectral measurements (Fluoromax-4, Horiba Scientific, Edison, NJ, USA). Excitation spectra were collected at 520 nm emission. Emission spectra were collected by exciting at 440 nm.

Electrophysiology. Whole cell voltage clamping measurements of 500 nM Bu_2N-TTz-Py labeled HEK 293T cells were performed with Axopatch 200A amplifier (Molecular Devices), digitized using an NI-6251 DAQ (National Instruments), and controlled using WinWCP software (Strathclyde Electrophysiology Software). Patch pipettes were pulled using a Sutter P-97

Micropipette puller. Patch pipettes with resistances between 5 - 10 MOhm were used in voltage clamping experiments. The patch pipette was positioned using an MP325 motorized manipulator (Sutter). Metamorph premier Ver. 7.8.12.0 was linked to an NI-6501 DAQ to enable voltage triggered image acquisition. Extracellular solution composition was 145 mM NaCl, 20 mM glucose, 10 mM HEPES, pH 7.4, 3 mM KCl, 2 mM $CaCl_2$, 1 mM $MgCl_2$ (310 mOsm); and the intracellular solution composition was 115 mM potassium gluconate, 10 mM EGTA tetrapotassium salt, 10 mM HEPES, pH 7.2, 5 mM NaCl, 10 mM KCl, 2 mM ATP disodium salt (290 mOsm).

Microscopy. Imaging was carried out on an IX83 inverted microscope (Olympus Corporation of the Americas, Center Valley, PA, USA) using 100X, 1.4 NA, DIC oil immersion objective (PLAPON, Olympus) and an Evolve Delta 512 EMCCD camera (Photometrics, USA). Filter wheel, shutter, and CCD camera were controlled using Metamorph premier Ver 7.8.12.0 (Molecular Devices, LLC, USA). For photostability studies, HEK 293T cells were labeled with 500 nM Bu_2N-TTz-Py and illuminated continuously with ~5 W/cm^2 power light source, periodically acquiring images at 1 min interval. Bu_2N-TTz-Py channel images were obtained using 480/20 bandpass excitation filter, 575/40 bandpass emission filter and 89016 dichroic. VF2.1.Cl channel images were obtained using 500/20 bandpass excitation filter, 535/40 bandpass emission filter and 69002 dichroic. For CellMaskTM red, images were obtained using the 640/30 bandpass excitation filter, 705/72 bandpass emission filter and 89016 dichroic.

Cellular localization: Time-lapse imaging was performed to probe the membrane localization of Bu_2N-TTz-Py at longer time scale. HEK 293T cells were labelled with 500 nM Bu_2N-TTz-Py and a plasma membrane marker (IX CellMask^{TM} Red, Thermofisher) for 10 mins in 1X HBSS (Hank's balanced salt solution, Thermofisher). Excess unbound dyes were washed with 1X PBS

and imaged after 30 mins incubation in 1X HBSS. The membrane localized Bu_2N-TTz-Py and CellMask™ Red were sequentially imaged every 20 mins. Intensity values at plasma membrane (I_{PM}) were calculated by drawing regions of interest (ROI) around the whole cell and subtracting intracellular intensity (I_{IM}, ROI drawn within the cell) for Bu_2N-TTz-Py and CellMask images, respectively. The normalized intensity ratio of Bu_2N-TTz-Py to CellMask™ Red, at plasma membrane (I_{PM} ratio) and intracellular membrane (I_{IM} ratio), were plotted w.r.t. time.

Cytotoxicity: Cellular toxicity of voltage sensitive dyes was characterized using Annexin V-Cy5 (BioVision) staining of phosphatidylserine that are exposed to outer leaflet of plasma membrane during apoptosis. HEK 293T cells were labelled with 500 nM of indicated dyes for 15 mins, followed by incubation with Annexin V-Cy5 for 20 mins in dark and washed, fixed with 4% paraformaldehyde before imaging. As a positive control, unlabeled HEK cells were incubated at 65°C for 10 mins to induce apoptosis and stained with Annexin V-Cy5 as above. Cytotoxicity percentage is calculated as number of Annexin V-Cy5 positive cells to total number of nuclear stained cells. Number of cells quantification were performed using Analyze particle function of ImageJ program.

2-(N,N-dibutyl-4-aminophenyl)-5-(4-pyridyl) thiazolo[5,4-d]thiazole (Bu_2N-TTz-Py): 4-Pyridinecarboxaldehyde (1.3401 g, 12.511 mmol), dithiooxamide (1.0007 g, 8.3253 mmol), and 4-(dibutylamino)benzaldehyde (2.9108 g, 12.474 mmol) were mixed in 40 mL anhydrous DMF for 6 h at 120 °C. After refrigerating overnight, a brownish-yellow powder precipitate was collected via vacuum filtration and rinsed with DMSO and water (1.374 g). Using a 1:1 hexanes:chloroform mixture, 31.4 mg of the crude product was purified by silica gel column chromatography (Silica Flash M60). The eluent was removed under vacuum, thereby yielding a yellow solid (2.3 mg, 2.9%). **^{1}H NMR** (500 MHz, CD_3CN, δ): 8.67 (d, J = 5.05 Hz, 2H), 7.84 (d,

J = 6.20 Hz, 2H), 7.79 (d, *J* = 9.15 Hz, 2H), 6.74 (d, *J* = 9.90 Hz, 2H). **^{13}C NMR** (126 MHz, DCM, protonated): 202.19, 197.48, 152.01, 142.06, 142.03. 141.96, 141.94, 129.87, 128.65, 121.66. **UV-Vis λ_{max} ($CHCl_3$, $M^{-1}cm^{-1}$):** 424 nm (ε = 17,700). **ESI-MS: calcd for $C_{23}H_{27}N_4S_2^+$, 423.1677; found, 423.1659.**

2-(N,N-diphenyl-4-aminophenyl)-5-(4-pyridyl) thiazolo[5,4-d]thiazole (Ph_2N-TTz-Py): 4-Pyridinecarboxaldehyde (0.2577 g, 2.406 mmol), dithiooxamide (0.2519 g, 2.0957 mmol), and 4-(diphenylamino)benzaldehyde (0.8634 g, 3.159 mmol) were mixed in 10 mL anhydrous DMF for 6 h at 120 °C. After sitting overnight, a brownish-yellow precipitate was collected via vacuum filtration and rinsed with water (0.3201 g). Using chloroform, 20.0 mg of the crude product was purified by silica gel column chromatography (Silica Flash M60). The eluent was removed under vacuum, thereby yielding a yellow solid (15.6 mg, 25.8%). **^{1}H NMR** (500 MHz, d-DMSO, δ): 8.72 (d, *J* = 5.48 Hz, 2H), 7.93 (d, *J* = 6.40 Hz, 2H), 7.89 (d, *J* = 8.70 Hz, 2H), 7.36 (m, 4H), 7.13 (m, 6H), 6.95 (d, *J* = 9.15 Hz, 2H). **^{13}C NMR** (126 MHz, DCM, protonated): 206.41, 152.86, 151.16, 150.83, 148.69, 148.63, 146.70, 129.61, 127.64, 126.21, 126.21, 125.76, 121.12, 120.28. **UV-Vis λ_{max} ($CHCl_3$, $M^{-1}cm^{-1}$):** 424 nm (ε = 46,400). **ESI-MS: calcd for $C_{27}H_{19}N_4S_2^+$, 463.1051; found, 463.0524.**

2-(N,N-diphenyl-4-aminophenyl)-5-(4-carboxyphenyl) thiazolo[5,4-d]thiazole (Ph_2N-TTz-COOH): 4-Formylbenzoic acid (0.3774 g, 2.514 mmol), dithiooxamide (0.2002 g, 1.666 mmol), and 4-(diphenylamino)benzaldehyde (0.6820 g, 2.495 mmol) were mixed in 16 mL anhydrous DMF for 6 h at 120 °C. The reaction mixture was cooled overnight, whereby a brownish-yellow solid precipitated out of solution. The precipitate was collected via vacuum filtration and rinsed with water (0.7044 g). Using chloroform, 21.7 mg of the precipitate was purified by silica gel column chromatography (Silica Flash M60). A yellow solid (6.3 mg, 24.3%) was collected after

chromatographic separation. **^{1}H NMR** (500 MHz, d-DMSO, δ): 8.10 (d, *J* = 8.70 Hz, 2H), 8.05 (d, *J* = 8.70 Hz, 2H), 7.88 (d, *J* = 8.70 Hz, 2H), 7.37 (m, 4H), 7.14 (m, 6H), 6.96 (d, J = 8.70 Hz, 2H). **^{13}C NMR** (126 MHz, DCM): 203.15, 146.97, 146.79, 144.46, 144.02, 136.09, 132.34, 130.33, 129.59, 127.47, 126.62, 125.66, 124.34, 122.90, 12132. **UV-Vis λ_{max} ($CHCl_3$, $M^{-1}cm^{-1}$):** 424 nm (ε = 13,900). **ESI-MS: calcd for $C_{29}H_{19}N_3O_2S_2$, 505.0919; found, 505.0991.**

2-(N,N-diphenyl-4-aminophenyl)-5-(4-formylphenyl) thiazolo[5,4-d]thiazole (Ph_2N-TTz-CHO): Terephthalaldehyde (0.3343 g, 2.49 mmol), dithiooxamide (0.2007 g, 1.67 mmol), and 4-(Diphenylamino)benzaldehyde (0.6824 g, 2.50 mmol), were refluxed in 10 mL of DMF for 6 h under aerobic conditions. The reaction mixture was allowed to sit overnight, and the precipitated product was collected by gravity filtration and rinsed with water (0.5046 g). A portion of the product (0.1994 g) was then purified by column chromatography on silica gel using hexanes/dichloromethane (10:1, 4:1) as eluent yielding a yellow solid (17.0 mg, 2.1%). **^{1}H NMR** (300 MHz, DCM, δ): 10.03 (s, 1H), 8.15 (d, *J* = 8.26 Hz, 2H), 7.95 (d, *J* = 8.52 Hz, 2H) 7.82 (d, *J* = 8.79 Hz, 2H), 7.31 (t, *J* = 8.79 Hz, 4H), 7.13 (t, *J* = 7.95 Hz, 6H), 7.05 (d, *J* = 8.79 Hz, 2H). **^{13}C NMR** (126 MHz, DCM): 191.29, 165.94, 152.09, 150.87, 150.56, 146.80, 141.11, 129.13, 137.36, 130.31, 129.59, 127.47, 126.61, 125.66, 124.3304, 121.33. **UV-vis λ_{max} (DCM, ε = M^{-1} cm^{-1}): 434 nm (ε = 35,100) ESI-MS: calcd for $C_{29}H_{20}N_3OS_2^+$: 490.1048; found, 490.1456.**

RESULTS AND DISCUSSION

The asymmetric, push-pull TTzs were accessed via one-pot syntheses which include, in each instance, a donor aromatic aldehyde (D-BzCHO), an acceptor aromatic aldehyde (A-BzCHO), and dithiooxamide. Initial asymmetric TTz reactions relied on modifying the literature procedure to accommodate a mixed-aldehyde approach, i.e. using an equivalent molar excess of

the aromatic aldehydes compared to dithiooxamide (3:2:3). Although accessed simply, the overall yields (2 - 26%) of the asymmetric TTzs (a-TTzs) were limited by the simultaneous formation of their symmetric counterparts (generalized within as D_2-TTz and A_2-TTz). The yields of Bu_2N-TTz-Py and Ph_2N-TTz-CHO were significantly lower than Ph_2N-TTz-Py and Ph_2N-TTz-COOH. In the case of Ph_2N-TTz-CHO, further reaction and polymerization of carboxaldehyde functionality likely hinders the overall yield. To better understand Bu_2N-TTz-Py synthesis, NMR studies were performed (see **Figure S29**) and show that the rates of reactivity of dibutylaminobenzaldehyde ($Bu_2NBzCHO$, the A-BzCHO) and pyridinecarboxaldehyde (PyBzCHO, the D-BzCHO) differ such that the formation of A_2-TTz is favored over a-TTz and D_2-TTz formation. It should be noted that the higher rate of reactivity of the D-BzCHO is congruent with analogous condensation reactions within the literature.[45] Another consequence of preferential D_2-TTz formation is that D-BzCHO may become the limiting reagent for the a-TTz reaction, thus leading to A_2-TTz becoming the secondary product. With these considerations in mind, the synthesis of Bu_2N-TTz-Py was studied by using an excess of the $Bu_2NBzCHO$ (1.25 to 1 to 5 mol ratio - PyBzCHO, dithiooxamide, $Bu_2NBzCHO$). NMR of the crude product shows a TTz ratio of 3:1:1 [Py_2-TTz, Bu_2N-TTz-Py, $(Bu_2N)_2$-TTz], significant amounts unreacted $Bu_2NBzCHO$ starting material, and impurities/side products. To inhibit the formation of side products, promote complete oxidation,[46] and encourage better final yields; the reaction was modified by reacting under N_2, adding dithiooxamide after heating to 120 °C, and oxidizing with DDQ after 4h of reaction time. According to an NMR of the crude product (**Figure S30)** the reaction proceeds more cleanly and results in a product ratio of 1.14 to 1 to 0.44 [Py_2-TTz, Bu_2N-TTz-Py, $(Bu_2N)_2$-TTz].

The absorption, emission, and fluorescence lifetime characteristics of all four TTz dyes were recorded in a variety of organic solvents (**Figure 2, Table 1**). Additionally, HOMO/LUMO levels of the TTz dyes were determined computationally in Spartan 16 using B3LYP/6-31g* (**Figure 2c, SI**). Molar absorptivities of all the TTz dyes ranged from 13,000 to 86,000 $cm^{-1}M^{-1}$. In comparison, the molar absorptivities of dipyridyl-TTz (in pyridine) and its alkylated derivatives (in H_2O) range from 32,000 to 46,000 $cm^{-1}M^{-1}$.[16] Interestingly, the peak molar absorptivities of Ph_2N-TTz-Py were two or more times greater than the peak molar absorptivities of both Bu_2N-TTz-Py and Ph_2N-TTz-COOH, while those of Ph_2N-TTz-CHO were over four-fold greater than Bu_2N-TTz-Py and Ph_2N-TTz-COOH in some solvents. TTz dyes containing the diphenyl substituted donor amine exhibited an increased molar absorptivity compared to the dibutyl substituted donor amine. However, the peak absorbance of Bu_2N-TTz-Py in DCM was slightly red-shifted as compared to that of Ph_2N-TTz-Py ($\lambda_{max, abs}$ = 429 nm vs $\lambda_{max, abs}$ = 422 nm in DCM), which is attributed to the diphenylamine moiety having weaker donor characteristics. The pyridyl and formylbenzyl acceptor moieties enhance the molar absorptivities of the TTz dyes relative to the benzoic acid TTz derivative Additionally, Ph_2N-TTz-CHO demonstrated the most red-shifted peak absorbance ($\lambda_{max, abs}$ = 434 nm in DCM), which is attributed to the 4-formylbenzyl moiety having stronger acceptor characteristics. Due to the low estimated ground state dipole moments of the TTz dyes (μ = 6 – 8 D), their wavelengths of absorbance remained relatively solvent independent (st. dev. = ±11 nm).[47]

The TTz dyes exhibit high quantum yields (QYs) in nonpolar solvents; however, as the polarity of the solvent increases, the emission intensities and, correspondingly, the QYs decrease (e.g. for Bu_2N-TTz-Py: Φ_{hex} = 0.93, Φ_{MeOH} = 0.04). The decrease in the QY is common for dyes with strong excited-state ICT character.[12, 48-49] In spite of having low QYs in polar solvents, the

TTz dyes could be expected to perform well in applications where they are localized to nonpolar environments (e.g. cell membranes); whereby their fluorescence would increase upon localization and any unlocalized dyes would contribute little background noise.[47]

TCSPC measurements of the TTz dyes show a general upward trend for fluorescent lifetimes as the polarity increases in aprotic solvents – from 1.50 – 1.89 ns in nonpolar solvents to ~3.00 ns in polar aprotic solvents (**Table 1**). The fluorescence lifetimes in protic solvents have the opposite trend; that is, a decrease in the fluorescence lifetime as the polarity increases (e.g. for Ph_2N-TTz-COOH: $\tau_{f,\ iPrOH}$ = 2.40 ns, $\tau_{f,\ MeOH}$ = 1.80 ns). The trend reversal in the fluorescence lifetime can most likely be attributed to the presence of hydrogen bonding in protic solvents. Due mostly to large changes in the QYs, but also to increasing fluorescent lifetimes in more polar aprotic solvents, the radiative rates (k_r) decrease relatively significantly with increasing solvent polarity. At the same time, the non-radiative rates of each TTz generally increases as solvent polarity increases. As with the asymmetric TTz dyes, it has been shown that neutral red (NR), another ICT dye, shows a similar trend.[50] Regardless, the fact that the fluorescence lifetimes are solvent dependent opens up the possibility of using these TTz dyes for measuring micelle formation and viscosity in living cells using fluorescence lifetime imaging (FLIM).[1, 51]

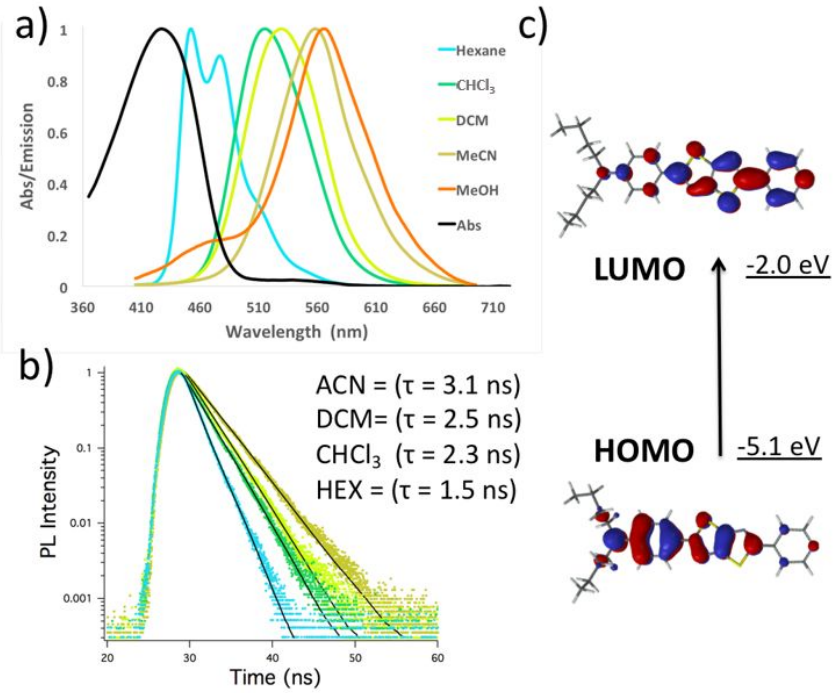

Figure 2. (a) Normalized UV-vis absorbance and solvent-dependent fluorescence, (b) solvent-dependent time-resolved fluorescence lifetimes, and (c) HOMO/LUMO molecular orbital configurations for Bu_2N-TTz-Py.

The presence of dual fluorescence and its dependence on solvent polarity is a well-documented phenomenon in many singly bonded D-A molecules with excited states that have highly dipolar quinoidal structures.[52] The higher frequency peak in nonpolar solvents can mostly be attributed to the locally excited (LE) state, whereas the lower frequency peak can mostly be attributed to the ICT state.[53] As is typically seen in similar D-A systems, it is suspected that the ICT state in the asymmetric TTz dye system is stabilized by the solvating effect of the polar solvent, thus causing the emission intensities of the dyes to broaden, diminish, and shift bathochromically with increasing solvent polarity. Another consequence of having electronically separated LE and ICT states is that the fluorescence lifetimes can increase in high-polar solvents even though the QYs are decreasing likewise; whereas, in typical non-ICT systems the fluorescence lifetimes and QYs are directly related.[47, 50]

Table 1. Optical Properties of TTz Dyes in Various Solvents

dye	solvent	Polarizability Factor Δf*	Abs (nm) λ_{max}	Abs (eV) E_{ex}	Ext. coeff. (M·cm)$^{-1}$ ε	Em (nm) λ_{max}	Em (eV) E_{em}	Stokes Shift SS (eV)	Φ_F	Fluorescence Lifetime (ns) τ_F	Radiative rate (sec^{-1}) k_r	Non-radiative rate (sec^{-1}) k_{nr}
	Hex	-0.00170	410	3.02	22000	450	2.76	0.27	0.93	1.50	6.2E+08	4.4E+07
Bu_2N	DCM	0.217	429	2.89	13000	515	2.41	0.48	0.35	2.47	1.4E+08	2.6E+08
-TTz-	$CHCl_3$	0.148	430	2.88	18000	532	2.33	0.55	0.45	2.26	2.0E+08	2.4E+08
Py	MeCN	0.305	425	2.92	20000	557	2.23	0.69	0.17	3.06	5.4E+07	2.7E+08
	MeOH	0.309	424	2.93	21000	565	2.20	0.73	0.04	1.23	3.1E+07	7.8E+08
	Tol	0.0132	419	2.96	36000	482	2.57	0.39	0.93	1.80	5.2E+08	3.9E+07
Ph_2N	DCM	0.217	422	2.94	34000	536	2.31	0.63	0.37	3.16	1.2E+08	2.0E+08
-TTz-	$CHCl_3$	0.148	424	2.93	46000	518	2.39	0.53	0.54	2.60	2.1E+08	1.8E+08
Py	EtOAc	0.199	415	2.99	48000	518	2.39	0.59	0.55	2.80	2.0E+08	1.6E+08
	Acetone	0.284	415	2.99	35000	554	2.24	0.75	0.17	2.70	6.3E+07	3.1E+08
	Tol	0.0132	424	2.93	22000	487	2.55	0.38	0.78	1.70	4.6E+08	1.3E+08
Ph_2N	DCM	0.217	424	2.93	21000	523	2.37	0.55	0.33	2.90	1.1E+08	2.3E+08
-TTz-	$CHCl_3$	0.148	425	2.92	14000	548	2.26	0.66	0.55	2.20	2.5E+08	2.0E+08
COOH	iPrOH	0.272	417	2.97	16000	522	2.38	0.60	0.37	2.40	1.5E+08	2.6E+08
	MeOH	0.309	414	3.00	17000	535	2.32	0.68	0.11	1.80	6.1E+07	4.9E+08
	Tol	0.0133	425	2.92	80230	501	2.48	0.44	0.72	1.89	3.8E+08	1.5E+08
Ph_2N	ClBz	0.143	436	2.84	18024	552	2.37	0.55	0.33	2.54	1.3E+08	2.6E+08
-TTz-	Cl_2Bz	0.186	440	2.82	37000	556	2.26	0.66	0.18	2.84	6.3E+07	2.9E+08
CHO	EtOAc	0.200	428	2.90	86081	548	2.26	0.63	0.36	3.09	4.2E+07	7.5E+07
	DCM	0.217	434	2.86	35100	560	2.21	0.64	0.13	2.40	1.5E+08	1.0E+09

*Solvents were chosen to span a wide range of polarizability factors ($\Delta f, see\ Eq.\ 1$). For direct comparisons, similar solvents were used when possible; however, solubility differences between the compounds prohibited complete standardization in this regard. To compensate, alternative solvents were selected based on solubility and Δf proximity. E.g. the diphenylamino TTzs were not soluble in hexanes ($\Delta f = -0.0017$), so toluene ($\Delta f = 0.013$) was chosen instead.

As shown in **Figure** 2 and listed in **Tabe 1**, the TTz dyes exhibit strong solvatofluorochromism – of which Bu_2N-TTz-Py shows the largest Stokes shift of the four TTz dyes (0.73 eV). The calculated HOMO/LUMO levels indicate that the strong solvatofluorochromism arises from an ICT mechanism, whereby the ground state has significant electron localization on the donor side of the molecule whereas the electron density shifts to the

acceptor moiety in the excited state. To more directly quantify the strong ICT character of the TTz dyes, the excited-state dipole moments were calculated using the Lippert-Mataga equation (**Eq 1**):

$$\nu_a - \nu_f = \frac{(\mu^* - \mu)^2}{4\pi\epsilon_0 hca^3}\Delta f + const. \quad ; \quad \Delta f = \left(\frac{\epsilon - 1}{2\varepsilon + 1} - \frac{\eta^2 - 1}{2\eta^2 + 1}\right)$$

where ν_a and ν_f are the wavenumbers of the absorption and emission peaks in cm^{-1}, respectively; μ^* and μ are the excited state and ground state dipoles, respectively; ϵ_0 is the vacuum permittivity, h is Planck's constant, c is the speed of light, a is the Onsager cavity radius, Δf is the orientation polarizability, ϵ is the relative permittivity, and η is the refractive index. The dipoles were calculated using Spartan 2016 software, and the Onsager cavity radius was calculated using Gaussian '09 software.

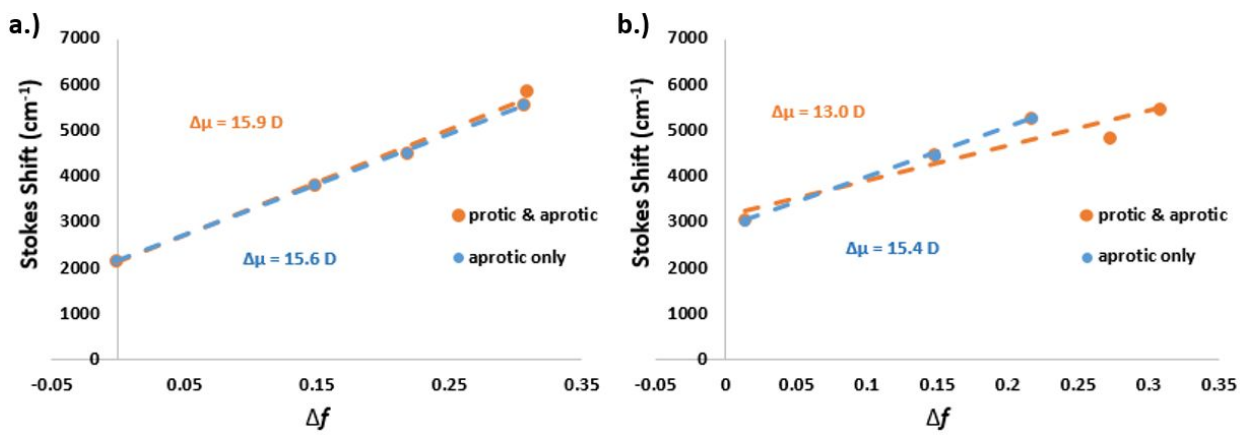

Figure 3. (a) Lippert-Mataga plots of Bu_2N-TTz-Py and (b) Ph_2N-TTz-COOH.

Figure 3 shows the Stokes shift of Bu_2N-TTz-Py and Ph_2N-TTz-COOH versus Δf. From the slopes of the Lippert-Mataga plots, the change between the dipole moments of the ground

and excited states can be determined. Even though the Lippert-Mataga equation assumes no specific solvent-solute interactions (e.g. hydrogen bonding) and ignores solute polarizability, high degrees of linearity are apparent, and therefore, the estimations of the excited state dipoles are regarded as reliable. Bu_2N-TTz-Py, in particular, shows a near unity correlation with Lippert-Mataga theory, thus suggesting minimal specific solvent-solute interactions and/or relatively rapid vibrational relaxation as compared to solvent relaxation.[11, 54-55] Perhaps owing to the minimal solvent interactions and rapid vibrational relaxation, the estimated changes in dipole moments ($\Delta\mu$) are remarkably large (**Table 2**). Bu_2N-TTz-Py, for example, has a calculated $\Delta\mu =$ 15.9 D and a $\mu^* =$ 24.3 D. Compared to similar small-molecule, push-pull dyes, the asymmetric TTz dyes have some of the largest ever reported $\Delta\mu$s – twice that of Prodan and comparable to FR0 and 7AHC.[12, 56] Therefore, it is expected that these asymmetric TTzs dyes would be well suited to give high sensitivity in sensing applications whereby small changes in the polarity of the environment can lead to large differences in the wavelengths of fluorescence.

Table 2. Ground and Excited State Dipole Moments

Compound	Onsager Cavity Radius a (Å)[a]	Ground State Dipole μ (D)[a]	Excited State Dipole μ^* (D)[b]	Change in Dipole $\Delta\mu$ (D)[b]
Bu_2N-TTz-Py	6.17	8.34	24.3	15.9
Ph_2N-TTz-Py	6.11	6.06	20.8	14.6
Ph_2N-TTz-COOH	6.16	8.36	21.3	13.0
Ph_2N-TTz-CHO	6.22	6.89	24.9	18.0

[a] Calculated using DFT B3LYP/6-31G(d) with tight SCF, finegrid integral, and volume keyword
[b] Semi-empirically calculated using the Lippert-Mataga Equation

In an extension of sensing the surrounding polarity, the dependence of the wavelength of emission as a function of temperature and pH were also explored (for pH studies see SI). For these efforts, Bu_2N-TTz-Py was chosen as a focal representative for our family of TTzs since it had the highest Stokes shift and otherwise similar photophysical characteristics. For the temperature studies, a 10 μM MeTHF solution of Bu_2N-TTz-Py was created and the emission of

the solution was monitored from -196 – 60 °C (see **Figure S2** for phosphorescence). MeTHF was chosen for its wide liquid temperature window and ability to form a glass upon freezing; most other solvents crystallize upon solidification and inhibit fluorescence. The low temperature studies were achieved using various liquid N_2 cooling baths (see Experimental). Due to the condensation of atmospheric moisture during low-temperature testing, only the normalized emission intensities are reported. As seen in **Figure 4**, Bu_2N-TTz-Py exhibits thermofluorochromism, whereby the wavelength of emission shifts bathochromically as temperature decreases (from 519 nm at 60 °C to 559 nm at -131 °C). At temperatures near the freezing point of MeTHF and below, however, the wavelength of emission rapidly blue-shifts from 559 to 544 to 503 nm at -131, -136, and -196 °C, respectively. Because the solvent polarity is dependent on the temperature of the solvent, the presence of thermofluorochromism could be fully expected, i.e. it is a direct analogue of solvatofluorochromism.[57] As a corollary, any solvent which also dissolves Bu_2N-TTz-Py will show a similar temperature affect; however, it is expected that the operable temperature range, sensitivity, and linearity would change correspondingly. Whereas as most dye systems demonstrate a hypsochromic shift upon temperature reduction, Bu_2N-TTz-Py demonstrates the opposite trend. General intuition might infer that the direct relationship between viscosity and temperature would likewise lead to faster solvation relaxation at higher temperatures and consequently red-shift the emission spectra. Higher temperatures, however, can also prevent the alignment of solvent dipoles, thus leading to a blue shift in the emission spectra as temperature increases – such as is seen for Bu_2N-TTz-Py and, previously, for Laurdan.[47, 58] Furthermore, the hypsochromic shift of the emission that was observed upon freezing is a well-known phenomenon, and can best be attributed to the complete inhibition of solvent relaxation effects upon freezing.[47] Nevertheless, to visualize the temperature

dependence of the emission wavelength, a temperature-wavelength correlation profile for Bu_2N-TTz-Py in MeTHF was created (**Figure 4**). It was observed that the wavelength of emission shows a strong linear correlation with the solution temperature while inside the temperature range in which MeTHF is liquid. Additionally, the TTz/MeTHF solution showed relatively high temperature sensitivity (-0.21 nm °C^{-1}), thus making it suitable for temperature sensing applications.[59-62]

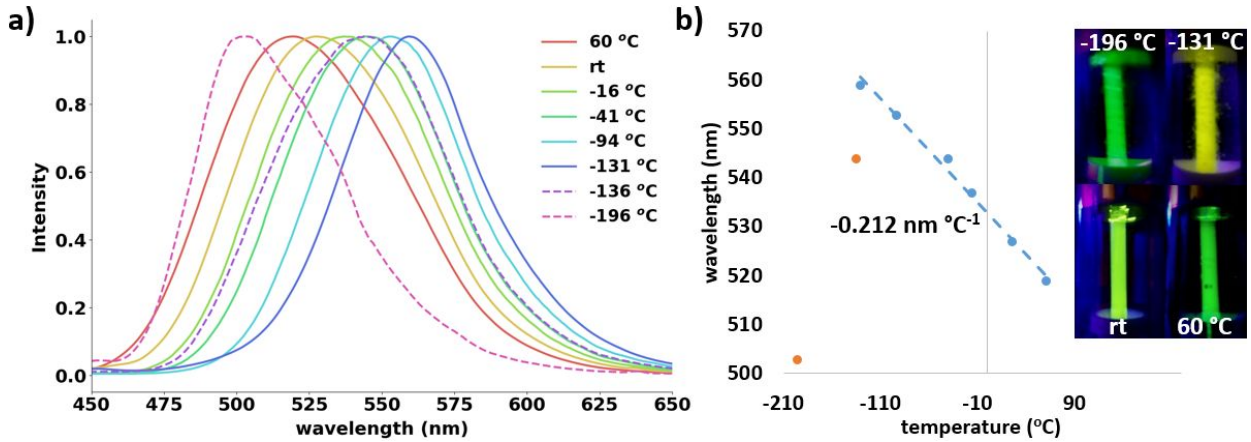

Figure 4. (a) Normalized emission intensity spectra of Bu_2N-TTz-Py and (b) temperature-wavelength correlation profile of Bu_2N-TTz-Py in MeTHF when T > -136 °C (blue) and T ≤ -136 °C (orange).

Having characterized the sensing capabilities of the asymmetric TTz dyes in solution, their efficacy as biologically relevant sensors was then explored via in vitro cell studies. Bu_2N-TTz-Py was selectively chosen based on its expected favorability toward membrane localization given its molecular structure (hydrophilic pyridyl head, hydrophobic dibutylamino tail). As shown in **Figures 5a/5b,** when Bu_2N-TTz-Py is applied to HEK 293T cells, the dye localizes to cell membranes, displaying peak excitation/emission wavelengths at 423 and 483 nm, respectively (**Figure 5c**). Also noteworthy, the wavelength of peak emission for Bu_2N-TTz-Py in

a solution of PBS with 0.1% Triton-X100 (518 nm) blue-shifts by 34 nm upon localizing to a cell membrane. A 34 nm blue shift is equivalent to the solvent polarity differential between DCM and toluene, thus further indicating that Bu_2N-TTz-Py intercalates between the phospholipid bilayer. Additionally, Bu_2N-TTz-Py has both poor solubility and low QY in aqueous environments resulting in low background fluorescence, which is visually apparent by the high amount of contrast between the cell membrane and its surrounding environment (**Figure 5b**). More conclusively, **Figures 5d/5e** show the time lapse imaging and quantification of localization of Bu_2N-TTz-Py in HEK 293T cells (6 independent experiments). Normalized against the fluorescence intensity of CellMask^{TM} red, a plasma membrane marker, the fluorescence intensities of the plasma membranes stained with Bu_2N-TTz-Py shows a 2.5% decrease after 50 min (26% decrease after 110 min). Given the brevity of the acquisition time (6 acquisitions per cell, 200 ms exposure per acquisition), the overall decrease of the plasma membrane fluorescence intensities of Bu_2N-TTz-Py is most likely not caused by photodegradation. Furthermore, the decrease of fluorescence intensities is not caused by dye internalization in any significant capacity since the normalized intensities of intracellular membranes stained with Bu_2N-TTz-Py indicate negligible TTz internalization (< 1% over 50 min, 5% over 130 min). It is therefore concluded that the majority of the fluorescence reduction after 50 min is caused by extracellular leaching.

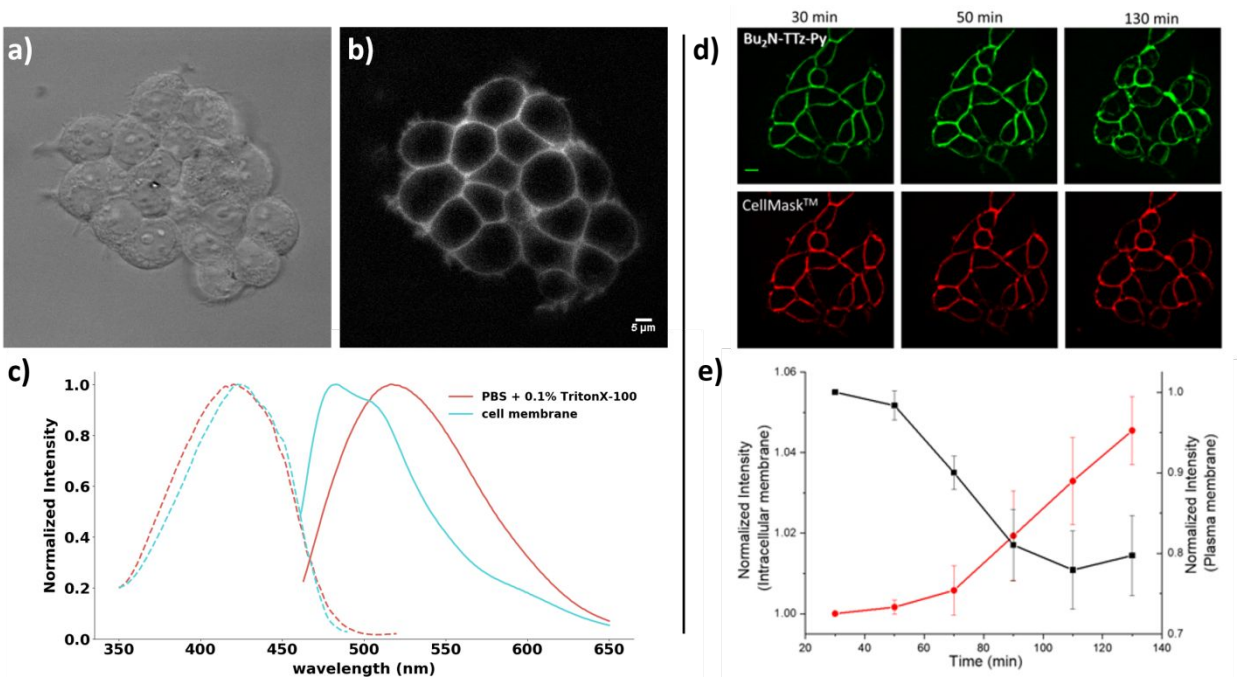

Figure 5. In vitro cellular characterization of Bu_2N-TTz-Py. (a, b) DIC and fluorescent images of HEK 293T cells labelled with 500 nM Bu_2N-TTz-Py in PBS buffer containing 0.01% Pluronic F127. (c) Normalized excitiation/emission spectra of 1 µM Bu_2N-TTz-Py in PBS buffer with 0.1% TritonX-100 before and after loading into ~0.5 x 10^5 J774.A1 cells. Exctitation spectra (- -) were collected at 520 nm and emission spectra (-) were collected with 440 nm exctiation. (d) Time lapse imaging of HEK 293T cells show partial internalization of Bu_2N-TTz-Py, but no internalization of CellMask stain after 130 min. (e) Quantification of intracellular membrane (red trace, circles) and plasma membrane (black trace, squares) localization of Bu_2N-TTz-Py over time. Error bars represent S.E.M. of 6 independent experiments. Scale bar = 10 µm.

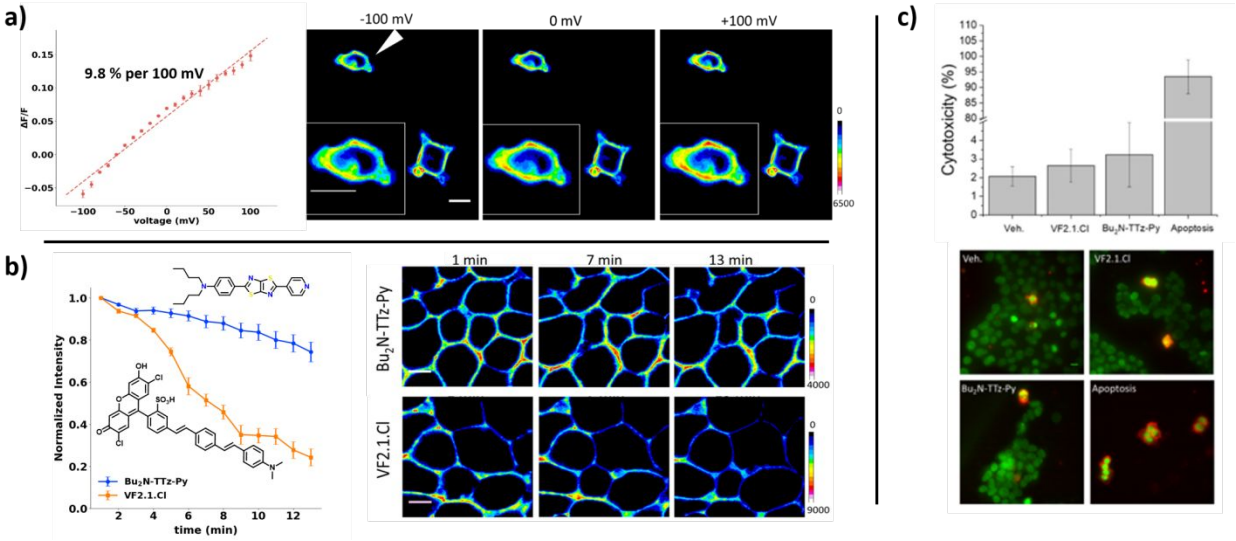

Figure 6. (a) Plot of fractional change in fluorescence (ΔF/F) vs clamped membrane potential of HEK 293T cells labelled with 500 nM Bu_2N-Py-TTz and representative pseudo-color images clamped at -100, 0, and +100 mV (shown by white arrow). Inset: Voltage clamped cell. (b) Photostability of Bu_2N-TTz-Py and VF2.1.Cl in HEK 293T cells (illuminated using λ = 440 nm at 5 W cm^{-2}) and their representative psuedo-color images under continous illumination at wavelength of maximum excitation. Error bars a/b represent the standard error of mean (S.E.M.) for 3 independent experiments, n = 12 total cells. Scale bar = 10 µm. (c) Annexin V-cy5 staining of HEK 293T cells incubated with DMSO (Veh.), VF2.1.Cl, Bu_2N-TTz-Py. Apoptosis for control (incubated cells 65 °C, 10 min). Percentages of cytotoxicity were calculated as number of 100 X Cy5 positive cells per number of nuclei stained. Error bars represent S.E.M. of three independent experiments, n = 250 cells. Scale bars = 10 µm.

Having established its environmental sensitivity and proclivity for membrane localization, it was hypothesized that Bu_2N-TTz-Py could orient itself favorably within cell membranes and sense voltage differentials across the membrane. To test the membrane voltage sensitivity of Bu_2N-TTz-Py, whole-cell patch clamp electrophysiology was performed on HEK 293T cells labeled with 500 nM Bu_2N-TTz-Py. As seen in **Figure 6a**, cells were held at -60 mV and stepped through 10 mV increments whereby depolarizing or hyperpolarizing voltage potentials resulted in either a florescence increase or decrease, respectively. Tests concluded that Bu_2N-TTz-Py has a voltage sensitivity of approximately 10% ΔF/F per 100 mV. For context, early generation VSDs, such as RH-421, ANNINE-6, and VF2.1.Cl, display maximum voltage sensitivities of 10% – 25% ΔF/F per 100 mV.[63-64] In other words, Bu_2N-TTz-Py shows a comparatively modest voltage sensitivity relative to comparable VSDs in the literature. It should also be noted that the voltage sensitivities, signal-to-noise, and linearity of VSDs with ICT character (e.g. Bu_2N-TTz-Py) can vary significantly depending on both the wavelength of excitation and probed emission.[65]

Encouraged by the promising voltage sensitivity data, the photostability of Bu_2N-TTz-Py was also tested and found to be much improved over the photostability of VF2.1.Cl (**Figure 5b**). Whereas VF2.1.Cl had a bleaching half-life of approximately 7.5 minutes under intense

illumination (I = 5 W cm^{-2}, ε = 22,300 cm^{-1} M^{-1} @ 440 nm LED[10]), the fluorescence intensity of Bu_2N-TTz-Py decayed by less than 10% in the same amount of time under identical conditions (ε = 15,000 – 20,000 cm^{-1} M^{-1} @ 440 nm LED). The improved photostability of Bu_2N-TTz-Py over that of VF2.1.Cl can best be attributed to the structural difference between both their head groups and bridging units. It is well known that fluorescein has low photostability and, in the case of VF2.1.Cl, it has been shown that derivitization of its fluorescein head group can drastically improve the photostability.[66-67] Additionally, p-phenylenevinylene (PPV), i.e. the bridging unit in VF2.1.Cl, has been shown to have photostability issues as well. [62-64] TTz, on the other hand, has excellent thermo-oxidative and photochemical stability. [25, 29] Furthermore, TTz has the added advantage of requiring only a single condensation step, whereas most other VSDs (including VF2.1.Cl) require multiple synthetic steps. However, the overall yields of the asymmetric TTz dyes and other VSDs remain similar.

Lastly, the cellular toxicities of Bu_2N-TTz-Py and VF2.1.Cl were characterized using Annexin V-Cy5 staining of phosphatidylserine. HEK 293T cells were labelled with Bu_2N-TTz-Py or VF2.1.Cl for 15 min, incubated with Annexin V-Cy5 for 20 min in the dark, washed, and fixed with 4% paraformaldehyde before imaging. As a positive control, apoptosis was induced via high-temperature incubation (65 °C, 10 min). As shown in **Figure 5c**, the treatments of Bu_2N-TTz-Py or VF2.1.Cl to HEK 293T cells both show insignificant cytotoxicity.

CONCLUSION

In conclusion, we have developed a family of asymmetric TTz dyes which exhibit remarkable solvatofluorochromism as a consequence of the unique structural features provided by the TTz core, namely its enhanced rigidity and planarity in which typical conjugated,

hydrocarbon bridges do not confer. Spectroscopic studies of these TTz dyes reveal large absorption coefficients, high quantum yields in nonpolar environments, significant Stokes shifts, and red-shifted absorption/emission peaks across a wide solvent range. Lippert-Mataga plots indicate that these TTz dyes have some of the largest dipole moments ever reported ($\Delta\mu$ = 13 – 18 D) - double that of Prodan and comparable to FR0 and 7AHC. Additionally, we have showed that the remarkable photophysical properties of the fused, bicyclic thiazolothiazole π-bridge make them ideal for polarity and/or temperature sensing applications. Furthermore, electrophysiological, in vitro cell studies indicate promising voltage sensitivities, negligible cytotoxicity, and photostabilities 4 times higher than that of VF2.1.Cl. Thus, the strong ICT character and remarkable photophysical properties of these new asymmetric TTz dyes make them attractive for a wide range of sensing applications.

ASSOCIATED CONTENT

Supporting Information

The Supporting Information is available free of charge on the ACS Publications website at DOI:

Optical band gaps, absorption and emission spectra, phosphorescence spectrum, DFT, TD-DFT, electrostatic potential maps, and all spectrophotometric titration information.

AUTHOR INFORMATION

Corresponding Author

*Michael.Walter@uncc.edu

ORCID

Michael G. Walter: 0000-0002-9724-265X

Notes

The authors declare no competing financial interests.

ACKNOWLEDGMENTS

This research was funded by the Department of Chemistry at the University of North Carolina at Charlotte, the B.S. Chemistry Program, and the Nanoscale Science Ph.D. program. MGW also acknowledges ACS Project SEED, Charlotte Research Scholars, and NSF-REU/DOD-ASSURE (CHE-1460867). Special thanks for research assistance from Brandon Miller, Jackson Mower, Jon Palmer, Mirna Peralta, Sashank Sabbineni, Natalie Herr, and Andrew Hyunn.

REFERENCES

1. Klymchenko, A. S., Solvatochromic and Fluorogenic Dyes as Environment-Sensitive Probes: Design and Biological Applications. *Acc. Chem. Res.* **2017,** *50* (2), 366-375.
2. Kumar, M.; Kumar, A.; Singh, M. K.; Sahu, S. K.; John, R. P., A novel benzidine based Schiff base "turn-on" fluorescent chemosensor for selective recognition of Zn2+. *Sensor Actuat B-Chem* **2017,** *241*, 1218-1223.
3. Liu, Z.; He, W.; Guo, Z., Metal coordination in photoluminescent sensing. *Chem. Soc. Rev.* **2013,** *42* (4), 1568-1600.
4. Yang, Y.-S.; Ma, C.-M.; Zhang, Y.-P.; Xue, Q.-H.; Ru, J.-X.; Liu, X.-Y.; Guo, H.-C., A highly selective "turn-on" fluorescent sensor for zinc ion based on a cinnamyl pyrazoline derivative and its imaging in live cells. *Anal. Methods* **2018,** *10* (16), 1833-1841.
5. Narayanaswamy, N.; Chakraborty, K.; Saminathan, A.; Zeichner, E.; Leung, K.; Devany, J.; Krishnan, Y., A pH-correctable, DNA-based fluorescent reporter for organellar calcium. *Nature Methods* **2019,** *16* (1), 95-102.
6. Liu, F.; Tang, Y.; Kuang, Y.; Pan, D.; Liu, X.; Yu, R.-Q.; Jiang, J.-H., An activatable fluorescent probe with an ultrafast response and large Stokes shift for live cell bioimaging of hypochlorous acid. *RSC Adv.* **2016,** *6* (109), 107910-107915.
7. Yang, X.; He, L.; Xu, K.; Yang, Y.; Lin, W., The development of an ICT-based formaldehyde-responsive fluorescence turn-on probe with a high signal-to-noise ratio. *New J. Chem.* **2018,** *42* (15), 12361-12364.
8. Ermakova, Y. G.; Sen, T.; Bogdanova, Y. A.; Smirnov, A. Y.; Baleeva, N. S.; Krylov, A. I.; Baranov, M. S., Pyridinium Analogues of Green Fluorescent Protein Chromophore: Fluorogenic Dyes with Large Solvent-Dependent Stokes Shift. *J. Phys. Chem. Lett.* **2018,** *9* (8), 1958-1963.
9. Niko, Y.; Didier, P.; Mely, Y.; Konishi, G.-i.; Klymchenko, A. S., Bright and photostable push-pull pyrene dye visualizes lipid order variation between plasma and intracellular membranes. *Sci. Rep.* **2016,** *6*, 18870.

10. Miller, E. W.; Lin, J. Y.; Frady, E. P.; Steinbach, P. A.; Kristan, W. B.; Tsien, R. Y., Optically monitoring voltage in neurons by photo-induced electron transfer through molecular wires. *Proc. Natl. Acad. Sci. U. S. A.* **2012,** *109* (6), 2114-2119.
11. Zhu, L.; Younes, A. H.; Yuan, Z.; Clark, R. J., 5-Arylvinylene-2,2′-bipyridyls: Bright "push–pull" dyes as components in fluorescent indicators for zinc ions. *J. Photoche. Photobiol., A: Chem.* **2015,** *311*, 1-15.
12. Kucherak, O. A.; Didier, P.; Mély, Y.; Klymchenko, A. S., Fluorene Analogues of Prodan with Superior Fluorescence Brightness and Solvatochromism. *J. Phys. Chem. Lett.* **2010,** *1* (3), 616-620.
13. Niko, Y.; Kawauchi, S.; Konishi, G.-i., Solvatochromic Pyrene Analogues of Prodan Exhibiting Extremely High Fluorescence Quantum Yields in Apolar and Polar Solvents. *Chem. Eur. J.* **2013,** *19* (30), 9760-9765.
14. Yamaguchi, K.; Murai, T.; Hasegawa, S.; Miwa, Y.; Kutsumizu, S.; Maruyama, T.; Sasamori, T.; Tokitoh, N., 5-N-Arylaminothiazoles as Highly Twisted Fluorescent Monocyclic Heterocycles: Synthesis and Characterization. *J. Org. Chem.* **2015,** *80* (21), 10742-10756.
15. Dell'Acqua, M.; Ronda, L.; Piano, R.; Pellegrino, S.; Clerici, F.; Rossi, E.; Mozzarelli, A.; Gelmi, M. L.; Abbiati, G., MediaChrom: Discovering a Class of Pyrimidoindolone-Based Polarity-Sensitive Dyes. *J. Org. Chem.* **2015,** *80* (21), 10939-10954.
16. Woodward, A. N.; Kolesar, J. M.; Hall, S. R.; Saleh, N.-A.; Jones, D. S.; Walter, M. G., Thiazolothiazole Fluorophores Exhibiting Strong Fluorescence and Viologen-Like Reversible Electrochromism. *J. Am. Chem. Soc.* **2017,** *139* (25), 8467-8473.
17. Luo, J.; Hu, B.; Debruler, C.; Liu, T. L., A π-Conjugation Extended Viologen as a Two-Electron Storage Anolyte for Total Organic Aqueous Redox Flow Batteries. *Angew. Chem. Int. ed.* **2018,** *57* (1), 231-235.
18. Nazim, M.; Ameen, S.; Shaheer Akhtar, M.; Shin, H.-S., D-π-A-π-D type thiazolo[5,4-d]thiazole-core organic chromophore and graphene modified PEDOT:PSS buffer layer for efficient bulk heterojunction organic solar cells. *Sol. Energy* **2018,** *171*, 366-373.
19. Roy, I.; Bobbala, S.; Zhou, J.; Nguyen, M. T.; Nalluri, S. K. M.; Wu, Y.; Ferris, D. P.; Scott, E. A.; Wasielewski, M. R.; Stoddart, J. F., ExTzBox: A Glowing Cyclophane for Live-Cell Imaging. *J. Am. Chem. Soc.* **2018,** *140* (23), 7206-7212.
20. Reginato, G.; Mordini, A.; Zani, L.; Calamante, M.; Dessì, A., Photoactive Compounds Based on the Thiazolo[5,4-d]thiazole Core and Their Application in Organic and Hybrid Photovoltaics. *Eur. J. Org. Chem.* **2016,** *2016* (2), 233-251.
21. Dessi, A.; Calamante, M.; Mordini, A.; Peruzzini, M.; Sinicropi, A.; Basosi, R.; Fabrizi de Biani, F.; Taddei, M.; Colonna, D.; Di Carlo, A.; Reginato, G.; Zani, L., Organic dyes with intense light absorption especially suitable for application in thin-layer dye-sensitized solar cells. *Chem. Commun.* **2014,** *50* (90), 13952-13955.
22. Subramaniyan, S.; Xin, H.; Kim, F. S.; Murari, N. M.; Courtright, B. A. E.; Jenekhe, S. A., Thiazolothiazole Donor–Acceptor Conjugated Polymer Semiconductors for Photovoltaic Applications. *Macromol.* **2014,** *47* (13), 4199-4209.
23. Dessì, A.; Barozzino Consiglio, G.; Calamante, M.; Reginato, G.; Mordini, A.; Peruzzini, M.; Taddei, M.; Sinicropi, A.; Parisi, M. L.; Fabrizi de Biani, F.; Basosi, R.; Mori, R.; Spatola, M.; Bruzzi, M.; Zani, L., Organic Chromophores Based on a Fused Bis-Thiazole Core and Their Application in Dye-Sensitized Solar Cells. *Eur. J. Org. Chem.* **2013,** *2013* (10), 1916-1928.

24. Zhang, M.; Guo, X.; Wang, X.; Wang, H.; Li, Y., Synthesis and Photovoltaic Properties of D–A Copolymers Based on Alkyl-Substituted Indacenodithiophene Donor Unit. *Chem. Mater.* **2011,** *23* (18), 4264-4270.
25. Saito, M.; Osaka, I.; Suzuki, Y.; Takimiya, K.; Okabe, T.; Ikeda, S.; Asano, T., Highly Efficient and Stable Solar Cells Based on Thiazolothiazole and Naphthobisthiadiazole Copolymers. *Sci. Rep.* **2015,** *5*, 14202.
26. Amina Khatun, D. K. P. N. S. M. G. W. S. S., Thiazolothiazole-Based Luminescent Metal–Organic Frameworks with Ligand-to-Ligand Energy Transfer and Hg2+-Sensing Capabilities. *Inorganic Chemistry*.
27. Ando, S.; Nishida, J.-i.; Inoue, Y.; Tokito, S.; Yamashita, Y., Synthesis, physical properties, and field-effect transistors of novel thiophene/thiazolothiazole co-oligomers. *J. Mater. Chem.* **2004,** *14* (12), 1787-1790.
28. Cheng, C.; Yu, C.; Guo, Y.; Chen, H.; Fang, Y.; Yu, G.; Liu, Y., A diketopyrrolopyrrole-thiazolothiazole copolymer for high performance organic field-effect transistors. *Chem. Commun.* **2013,** *49* (20), 1998-2000.
29. Yan, L.; Zhao, Y.; Wang, X.; Wang, X.-Z.; Wong, W.-Y.; Liu, Y.; Wu, W.; Xiao, Q.; Wang, G.; Zhou, X.; Zeng, W.; Li, C.; Wang, X.; Wu, H., Platinum-Based Poly(Aryleneethynylene) Polymers Containing Thiazolothiazole Group with High Hole Mobilities for Field-Effect Transistor Applications. *Macromol. Rapid Commun.* **2012,** *33* (6-7), 603-609.
30. Osaka, I.; Zhang, R.; Liu, J.; Smilgies, D.-M.; Kowalewski, T.; McCullough, R. D., Highly Stable Semiconducting Polymers Based on Thiazolothiazole. *Chem. Mater.* **2010,** *22* (14), 4191-4196.
31. Dessì, A.; Calamante, M.; Mordini, A.; Peruzzini, M.; Sinicropi, A.; Basosi, R.; Fabrizi de Biani, F.; Taddei, M.; Colonna, D.; di Carlo, A.; Reginato, G.; Zani, L., Thiazolo[5,4-d]thiazole-based organic sensitizers with strong visible light absorption for transparent, efficient and stable dye-sensitized solar cells. *RSC Adv.* **2015,** *5* (41), 32657-32668.
32. Kudrjasova, J.; Herckens, R.; Penxten, H.; Adriaensens, P.; Lutsen, L.; Vanderzande, D.; Maes, W., Direct arylation as a versatile tool towards thiazolo[5,4-d]thiazole-based semiconducting materials. *Org. Biomol. Chem.* **2014,** *12* (26), 4663-4672.
33. Nazim, M.; Ameen, S.; Akhtar, M. S.; Seo, H.-K.; Shin, H. S., Novel liquid crystalline oligomer with thiazolothiazole-acceptor for efficient BHJ small molecule organic solar cells. *Syn. Met.* **2014,** *187*, 178-184.
34. Dessì, A.; Calamante, M.; Mordini, A.; Peruzzini, M.; Sinicropi, A.; Basosi, R.; Fabrizi de Biani, F.; Taddei, M.; Colonna, D.; Di Carlo, A.; Reginato, G.; Zani, L., Organic dyes with intense light absorption especially suitable for application in thin-layer dye-sensitized solar cells. *Chem. Commun.* **2014,** *50* (90), 13952-13955.
35. Zani, L.; Reginato, G.; Mordini, A.; Calamante, M.; Peruzzini, M.; Taddei, M.; Sinicropi, A.; Parisi, M. L.; Fabrizi de Biani, F.; Basosi, R.; Cavallaro, A.; Bruzzi, M., An unusual thiazolo[5,4-d]thiazole sensitizer for dye-sensitized solar cells. *Tetrahedron Lett.* **2013,** *54* (30), 3944-3948.
36. Kudrjasova, J.; Kesters, J.; Verstappen, P.; Brebels, J.; Vangerven, T.; Cardinaletti, I.; Drijkoningen, J.; Penxten, H.; Manca, J.; Lutsen, L.; Vanderzande, D.; Maes, W., A direct arylation approach towards efficient small molecule organic solar cells. *J. Mater. Chem. A* **2016,** *4* (3), 791-795.

37. Benin, V.; Yeates, A. T.; Dudis, D., Preparation of halogenated derivatives of thiazolo[5,4-d]thiazole via direct electrophilic aromatic substitution. *J. Heterocyclic Chem.* **2009,** *45* (3), 811-819.
38. Ziessel, R.; Nano, A.; Heyer, E.; Bura, T.; Retailleau, P., Rational Design of New Thiazolo-Thiazole Dyes as Input Energy Units in Molecular Dyads. *Chem. Eur. J.* **2013,** *19* (8), 2582-2588.
39. Weber, G.; Farris, F. J., Synthesis and spectral properties of a hydrophobic fluorescent probe: 6-propionyl-2-(dimethylamino)naphthalene. *Biochemistry.* **1979,** *18* (14), 3075-3078.
40. Brouwer, A. M., Standards for photoluminescence quantum yield measurements in solution (IUPAC Technical Report). *Pure and Applied Chemistry* **2011,** *83* (12), 2213-2228-2228.
41. Suzuki, K.; Kobayashi, A.; Kaneko, S.; Takehira, K.; Yoshihara, T.; Ishida, H.; Shiina, Y.; Oishi, S.; Tobita, S., Reevaluation of absolute luminescence quantum yields of standard solutions using a spectrometer with an integrating sphere and a back-thinned CCD detector. *Physical Chemistry Chemical Physics* **2009,** *11* (42), 9850-9860-9860.
42. Axel, D. B., Density-functional thermochemistry. III. The role of exact exchange. *J Chem Phys 98*, 5648-5652.
43. P J Stephens, F. J. D. C. F. C. M. J. F., Ab Initio Calculation of Vibrational Absorption and Circular Dichroism Spectra Using Density Functional Force Fields. *The Journal of Physical Chemistry 98*, 11623-11627.
44. W J Hehre, R. D. J. A. P., Self—Consistent Molecular Orbital Methods. XII. Further Extensions of Gaussian—Type Basis Sets for Use in Molecular Orbital Studies of Organic Molecules. *J Chem Phys 56*, 2257-2261.
45. Yohei Ogiwara, K. T. T. K. N. S., Indium(III)-Catalyzed Knoevenagel Condensation of Aldehydes and Activated Methylenes Using Acetic Anhydride as a Promoter. *J Org Chem* **2015,** *80*, 3101-3110.
46. G Reginato, A. M. L. Z. M. C. A. D., Photoactive Compounds Based on the Thiazolo 5,4-d thiazole Core and Their Application in Organic and Hybrid Photovoltaics. *European Journal of Organic Chemistry 2016*, 233-251.
47. Lakowicz, J. R., *Principles of Fluorescence Spectroscopy*. Springer: Baltimore, 2006.
48. Bhattacharyya, K.; Chowdhury, M., Environmental and magnetic field effects on exciplex and twisted charge transfer emission. *Chemical Reviews* **1993,** *93* (1), 507-535-535.
49. Soujanya, T.; Fessenden, R. W.; Samanta, A., Role of Nonfluorescent Twisted Intramolecular Charge Transfer State on the Photophysical Behavior of Aminophthalimide Dyes. *The Journal of Physical Chemistry* **1996,** *100* (9), 3507-3512.
50. Singh, M. K.; Pal, H.; Bhasikuttan, A. C.; Sapre, A. V., Dual Solvatochromism of Neutral Red. *Photochemistry and Photobiology* **1998,** *68* (1), 32-38.
51. Mallick, S.; Pal, K.; Koner, A. L., Probing microenvironment of micelle and albumin using diethyl 6-(dimethylamino)naphthalene-2,3-dicarboxylate: An electroneutral solvatochromic fluorescent probe. **2016,** *467*.
52. Grabowski, Z. R.; Rotkiewicz, K.; Rettig, W., Structural Changes Accompanying Intramolecular Electron Transfer: Focus on Twisted Intramolecular Charge-Transfer States and Structures. *Chemical Reviews* **2003,** *103* (10), 3899-4032.
53. Hu, R.; Lager, E.; Aguilar-Aguilar, A. l.; Liu, J.; Lam, J. W. Y.; Sung, H. H. Y.; Williams, I. D.; Zhong, Y.; Wong, K.; Peña-Cabrera, E.; Tang, B., Twisted Intramolecular

Charge Transfer and Aggregation-Induced Emission of BODIPY Derivatives. *The Journal of Physical Chemistry C* **2009,** *113* (36), 15845-15853.
54. E, L., Zeitschrift für physikalische Chemie. *Zeitschrift für physikalische Chemie.* **1956,** *6*, 125.
55. Mataga, N.; Kaifu, Y.; Koizumi, M., *Solvent Effects upon Fluorescence Spectra and the Dipolemoments of Excited Molecules*. 1956; Vol. 29, p 465-470.
56. Giordano, L.; Shvadchak, V. V.; Fauerbach, J. A.; Jares-Erijman, E. A.; Jovin, T. M., Highly Solvatochromic 7-Aryl-3-hydroxychromones. *The Journal of Physical Chemistry Letters* **2012,** *3* (8), 1011-1016.
57. Reichardt, C., Solvatochromism, thermochromism, piezochromism, halochromism, and chiro-solvatochromism of pyridinium N -phenoxide betaine dyes. *Chemical Society Reviews* **1992,** *21* (3), 147-153-153.
58. Viard, M.; Gallay, J.; Vincent, M.; Meyer, O.; Robert, B.; Paternostre, M., Laurdan solvatochromism: solvent dielectric relaxation and intramolecular excited-state reaction. *Biophysical Journal* **1997,** *73* (4), 2221-2234-2234.
59. Seeboth, A.; Kriwanek, J.; Vetter, R., The first example of thermochromism of dyes embedded in transparent polymer gel networks. *Journal of Materials Chemistry* **1999,** *9* (10), 2277-2278-2278.
60. Chen, K.; Catalano, V. J., Luminescent Thermochromism in a Gold(I)–Copper(I) Phosphine–Pyridine Complex. *European Journal of Inorganic Chemistry* **2015,** *2015* (31), 5254-5261-5261.
61. Burt, M. C.; Dave, B. C., An optical temperature sensing system based on encapsulation of a dye molecule in organosilica sol–gels. *Sensors and Actuators B: Chemical* **2005,** *107* (2), 552-556-556.
62. Bacci, M.; Brenci, M.; Conforti, G.; Falciai, R.; Mignani, A. G.; Scheggi, A. M., Thermochromic transducer optical fiber thermometer. *Applied Optics* **1986,** *25* (7), 1079.
63. Huang, Y.-L.; Walker, A. S.; Miller, E. W., A Photostable Silicon Rhodamine Platform for Optical Voltage Sensing. *Journal of the American Chemical Society* **2015**.
64. Kuhn, B.; Fromherz, P., Anellated Hemicyanine Dyes in a Neuron Membrane: Molecular Stark Effect and Optical Voltage Recording. *The Journal of Physical Chemistry B* **2003,** *107* (31), 7903-7913.
65. Kuhn, B.; Roome, C. J., Primer to Voltage Imaging With ANNINE Dyes and Two-Photon Microscopy. *Frontiers in Cellular Neuroscience* **2019,** *13*, 321.
66. Whitaker, J. E.; Haugland, R. P.; Ryan, D.; Hewitt, P. C.; Haugland, R. P.; Prendergast, F. G., Fluorescent rhodol derivatives: Versatile, photostable labels and tracers. *Analytical Biochemistry* **1992,** *207* (2), 267-279.
67. Kulkarni, R. U.; Kramer, D. J.; Pourmandi, N.; Karbasi, K.; Bateup, H. S.; Miller, E. W., Voltage-sensitive rhodol with enhanced two-photon brightness. *Proceedings of the National Academy of Sciences* **2017,** *114* (11), 2813-2818.

For Table of Contents Only: